CHIN. PHYS. LETT. Vol. 36, No. 1 (2019) 015201

Electron Magnetohydrodynamics Magnetic Reconnection Experiment on Keda Linear Magnetized Plasma Device *

Feibin Fan(范费彬)[1], Jinlin Xie(谢锦林)[2**], Qiaofeng Zhang(张乔枫)[2],
Longlong Sang(桑龙龙)[1], Weixing Ding(丁卫星)[1]

[1]*CAS Key Laboratory of Geoscience Environment, School of Earth and Space Sciences, University of Science and Technology of China, Hefei 230026*
[2]*CAS Key Laboratory of Geoscience Environment, School of Physics, University of Science and Technology of China, Hefei 230026*

(Received 28 June 2018)

We conduct an electron magnetohydrodynamics magnetic reconnection experiment with guide-field in our Keda linear magnetized plasma device, in which two pulsed currents with the same direction are conducted in parallel with the axial direction of the main chamber of the device using two long aluminum sticks. After approximately 5 μs, an X-type magnetic field line topology is formed at the center of the chamber. With the formation of the X-type topology of magnetic field lines, we can also find the rapid increase of the current and ratio of the common flux to the private flux in this area. Additionally, a reduction in the plasma density and the plasma density concentration along one pair of separatrices can also be found.

PACS: 52.35.Vd, 52.25.−b, 94.30.cp DOI: 10.1088/0256-307X/36/1/015201

The source energy for explosive phenomena that occur in astrophysical and space plasmas, including stellar flares and substorms in the Earth's magnetosphere, is considered to come from the magnetic field.[1,2] However, a physical mechanism for rapid conversion of magnetic energy into plasma kinetic energy is required to explain these explosive phenomena. Magnetic reconnection, which is accompanied by reorganization of the magnetic field lines, provides this type of physical mechanism.[3,4] The two main tools used to study magnetic reconnection are satellites and theoretical analyses (including simulations), and great progress has been made in this field. It has been found that the reconnection rate in a collisionless magnetic reconnection process is high enough to account for the fast energy conversion that occurs during these explosive phenomena.[5,6] Collisionless magnetic reconnection is characterized by the quadrupole structure of the out-of-plane magnetic field,[5,7–13] along with the secondary islands that occur in the diffusion region.[14–17] Recently, electron-scale magnetic reconnection has also been observed by the magnetospheric multiscale mission.[18,19] Laboratory experiments provide another important way to study magnetic reconnection. When compared with satellite observation, laboratory experiments offer several advantages, including adjustable plasma parameters, repeatability and the availability of comprehensive diagnostics.[20]

With the continuing development of plasma technology, magnetic reconnection has been successfully performed in several well-designed laboratory experiments,[21] such as LCD, TS-3, the magnetic reconnection experiment (MRX) and the versatile toroidal facility (VTF). The LCD device has observed the existence of a current sheet and the heating of the electrons.[22,23] Experiments performed in TS-3 found that the reconnection rate decreased as the guide field became stronger.[24] A series of systematic magnetic reconnection experiments have been performed in the MRX device at Princeton University. These experiments verified the existence of the Hall effect in magnetic reconnection based on the quadrupolar structure of the out-of-plane magnetic field for the first time and they also indicated that the Hall effect plays an important role in fast reconnection.[25] Ion acceleration and heating during collisionless magnetic reconnection have also been observed and the influence of the boundary conditions has been studied.[26] It should be noted that in these laboratory experiments, the reconnections are all made in a controlled manner with external driving. Magnetic reconnection has also been realized in laser-driven plasma and electron acceleration has been observed.[27,28]

We have performed magnetic reconnection experiments on the Keda linear magnetized plasma (KLMP) device. First, we describe the experimental setup, and the results are then presented. A summary of the work and a discussion are then provided.

The scheme of the KLMP device is shown in Fig. 1, where the total length of the device is 280 cm. The vacuum chamber is 200 cm long, and it has a diameter of 25 cm. There are 12 sets of magnetic coils located around the vacuum chamber that work in a steady state and produce an axial magnetic field of 180–300 G to confine the plasma. The plasma source at the right end of the device is a 15-cm-diameter oxide-coated cathode with a 10-cm-diameter mesh anode. The working gas is argon at an operating pressure of $p_0 \approx 4 \times 10^{-2}$ Pa. The plasma source is operated in pulse mode at frequency of 1 Hz, and the pulse length is 12 ms. The typical plasma parameters are the electron number density $n_e \approx 2 \times 10^{12}\,\mathrm{cm}^{-3}$

*Supported by the National Natural Science Foundation of China under Grant Nos 41331067 and 41527804, the Key Research Program of Frontier Sciences of Chinese Academy of Sciences under Grant No QYZDJ-SSW-DQC010, and the Fundamental Research Funds for the Central Universities.
**Corresponding author. Email: jlxie@ustc.edu.cn
© 2019 Chinese Physical Society and IOP Publishing Ltd

and the plasma temperature $T_e \approx 10T_i \approx 4\,\text{eV}$ (where the subscripts i and e represent ion and electron, respectively). The electron mean free path is approximately $\lambda_e \approx 30\,\text{cm}$ longer than the characteristic device length $L \approx 10\,\text{cm}$, which means that the electron collisions are negligible. The ion and electron inertial lengths are $d_i \approx 1.5\,\text{m}$ and $d_e \approx 5\,\text{mm}$, respectively, which means that the experiment is performed in the ion diffusion region. Therefore, during our experiment, the electrons are magnetized ($d_e \ll L$) while the ions are not magnetized ($d_i \gg L$). The electrons in our experiment are thus collisionless and magnetized and can be treated as a magnetofluid, while the ions are not magnetized. This means that the reconnection occurring in our experiment is electron magnetohydrodynamics (EMHD) reconnection.

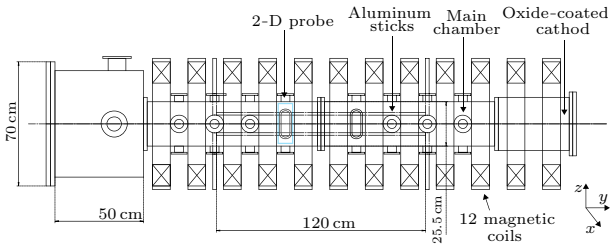


Fig. 1. A schematic view of the Keda linear magnetized plasma device.

Two 120-cm-long aluminum sticks are set parallel to the chamber at a distance of 10 cm, as shown in Fig. 2(a). Identical pulsed currents are conducted in these two sticks, and the induced magnetic fields have opposite directions in the middle of the chamber. The time evolution of the current is illustrated in Fig. 2(b). In this experiment, we focus only on the current rising phase. During the rising phase, the magnetic field increases and the magnetic field lines are 'pushed' from the two sticks towards the center as shown in Fig. 2(a), which drives the magnetic reconnection. With the existence of the axial magnetic field described above, the magnetic reconnection in our experiment is a driven guide-field reconnection. For the case presented in this work, the guide magnetic field is fixed at 180 G.

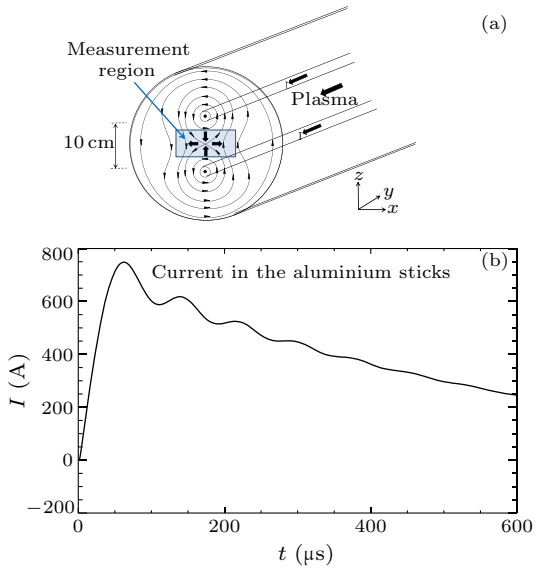


Fig. 2. (a) A cross-section view of the device showing the setup of the experiment and the geometry of the magnetic field. (b) The time evolution of the current in the sticks.

A two-dimensional continuously moving probe is used to scan the x–z section of the device. At the top of the probe shaft, two perpendicular magnetic coils are installed to diagnose the magnetic fields in the x and z directions, while a Langmuir probe is used to measure the ion saturation currents, which provide a good estimate of the plasma density. The scanning ranges are x=[−5 cm, 5 cm] and z=[−3 cm, 3 cm] (where the center of the two aluminum sticks is set to be (0, 0)), as shown in Fig. 2(a), and the data are collected at 21 × 13 grid points that are spaced 0.5 cm apart in both the x and z directions. Data from 10 pulses are collected at each grid point and are then averaged to reduce the overall noise. In this way, the magnetic field profile and the ion saturation current in the x–z section can be obtained.

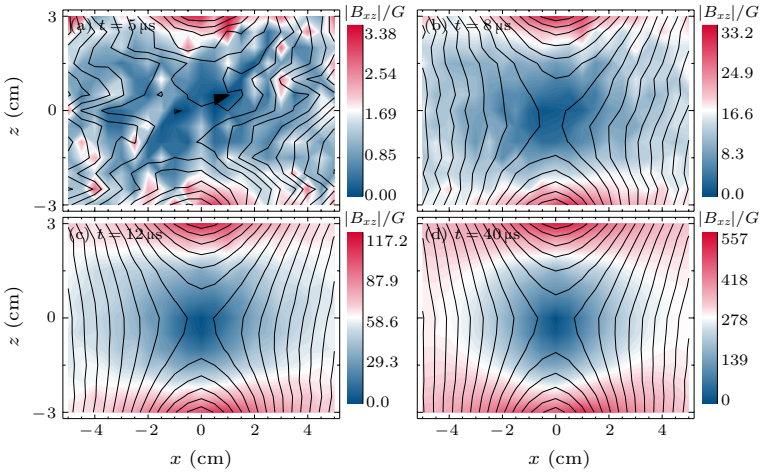


Fig. 3. The time evolution of the magnetic flux contours (black lines) and magnetic field in the x–z plane at (a) $t = 5\,\mu\text{s}$, (b) $t = 8\,\mu\text{s}$, (c) $t = 12\ \mu\text{s}$, and (d) $t = 40\,\mu\text{s}$.

In our experiment, we can estimate the components of magnetic flux in the x–z plane by integrating the magnetic field over the x–z sector, and the magnetic flux contours are then used to represent the magnetic field lines. In Fig. 3, we show the magnetic field lines and the magnetic field in the x–z plane at four different instants. Around the time of 5 μs, an X-type topology begins to form for the magnetic field lines, and this topology can be identified clearly from approximately 8 μs onwards. A structure of this type is a typical reconnection structure.

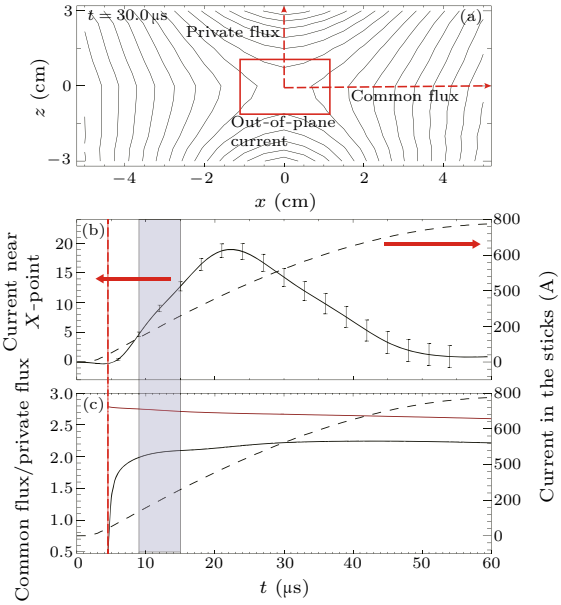


Fig. 4. (a) Integration path of (b) and (c). (b) The solid line represents the current near the X point that was obtained by integrating the magnetic field along the path indicated in (a), and the error bar was obtained by integrating the magnetic field along the same path that was used in the experiment performed in the vacuum. (c) The black solid line represents the ratio of the common flux to the private flux versus time, while the red solid line indicates the obtained common flux/private flux ratio versus time when no plasma is present in the device. The dashed lines shown in (b) and (c) represent the currents in the sticks for reference.

To determine whether or not a current sheet is formed in the region with the X-type magnetic field line topology, we calculate the current crossing the rectangle (3 cm×2 cm) indicated by the red lines shown in Fig. 4(a), and this current can be expressed as $I = \iint J_y dxdz = \iint (\nabla \times \boldsymbol{B})_y/\mu_0 dxdz = \oint 1/\mu_0 \boldsymbol{B} \cdot \delta \boldsymbol{l}$. Therefore, the current that crosses the rectangle can be calculated using the path integral along the rectangle's border. Figure 4(b) shows the time evolution of the current as it crosses the rectangle and the currents in the sticks are also plotted for reference. The current begins to increase at approximately 5 μs, when the X-type topology of the magnetic field lines was formed. At approximately 24 μs, the current reaches its maximum value of about 20 A before gradually being reduced to nearly zero at around 55 μs. At that stage, the rising phase of the current in the two sticks is almost complete. It is clearly shown that the current sheet appears simultaneously with formation of the X-type magnetic field line topology in the same region.

The ratio of the common flux to the private flux is generally used to describe magnetic reconnection quantitatively.[23] We also calculate this type of ratio during our experiment. The common flux is represented by integration of the magnetic flux along the line $z = 0$, from the X point to the edge of the diagnostic region; the private flux is given by integration of the magnetic flux along the line $x = 0$ from the X point to the edge of the diagnostic region and is shown as dashed lines in Fig. 4(a). The common flux is the magnetic flux after reconnection, while the private flux is the corresponding flux before reconnection, and the slope of the ratio of these two fluxes can partly represent the reconnection rate. Figure 4(c) depicts the evolution of the common flux/private flux ratio. The figure shows that from 5 μs, when the current in the region of interest (see Fig. 4(a)) begins to increase, the ratio of the common flux to the private flux also increases rapidly and then slows down again at approximately 12 μs. The ratio then gradually increases until it saturates at approximately 40 μs. This means that the reconnection is comparatively fast in the initial stages before it slows down and remains steady until 40 μs.

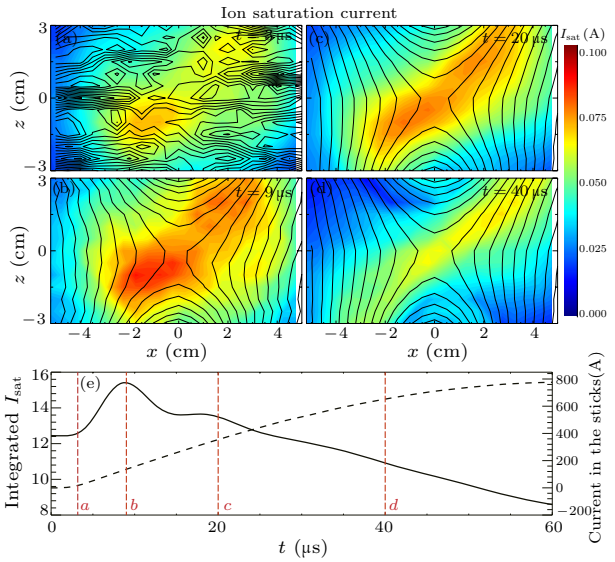


Fig. 5. Time evolution of ion saturation currents in the x–z plane at (a) $t = 3$ μs, (b) $t = 9$ μs, (c) $t = 20$ μs and (d) $t = 40$ μs. (e) The solid line represents the integration of the ion saturation currents over the entire diagnostic region and the black dashed line represents the current in the sticks for reference, while red dashed lines plot the times selected for a–d.

Figures 5(a)–5(d) show the time evolution of the ion saturation current profile, where the ion saturation current is proportional to the plasma density and its distribution can represent the plasma density contour. Initially, the plasma density distribution has a relatively uniform shape that is consistent with the emission from the cathode. At approximately 40 μs, the plasma density becomes concentrated along one pair of the separatrices. This type of distribution has also been observed by Frank *et al.*[29] and may be

caused by electric drift of ions in the guide-field reconnection and deviation of the plasma emitted from the cathode caused by the magnetic field. Figure 5(e) shows the evolution of the total ion saturation current, which is used to describe the total plasma density within the diagnostic region shown in Fig. 4(a). We see that the plasma density increases rapidly and reaches a peak at approximately 9 μs, when the X-type magnetic topology begins to form (5(a) and 5(b)). This is caused by squeezing of the plasma by the magnetic field that is generated by the current in the sticks. The total plasma density suddenly decreases in the time period between 9 μs and 15 μs (the shaded region in Fig. 4), which is possibly caused by ion outflow of the magnetic reconnection. In previous similar experiments,[21] it was reported that the ion outflow speed is around 0.1 of the Alfven speed because of the effects of the device boundaries. In our case, the Alfven speed in the reconnection region is about 35000 m/s (reconnection field $B \approx 100$ G and plasma density $n \approx 1 \times 10^{18}/\mathrm{m}^3$) which represents an ion outflow speed of approximately 3500 m/s. This means that the plasma may need a few μs to leave the region, which is consistent with the observed time period of the total plasma density reduction. After 20 μs, the X-type magnetic topology is formed and the plasma leaves the region along one pair of separatrices, which then leads to a reduction in the plasma density.

In conclusion, we have realized an EMHD magnetic reconnection experiment in our KLMP device. In this experiment, magnetic reconnection was driven using two parallel currents conducted by the two long aluminum sticks that were set parallel to the device chamber. With the appearance of the X-type magnetic field line topology at the center of the chamber, we also observed a rapid increase in the current. This means that the X-type magnetic field line topology is formed in an intense current sheet. Simultaneously, we also observed a rapid increase in the ratio of the common flux to the private flux and the concentration of the plasma along one pair of separatrices as the total plasma density decreases. All of the observed properties are consistent with those of magnetic reconnection, and we thus conclude that we observe magnetic reconnection in our KLMP device.

In this work, although we have realized magnetic reconnection in our KLMP device, we cannot measure the reconnection electric field and the electron and ion flows, which are highly important parameters in magnetic reconnection, because of the limited range of diagnostic tools that are currently available. We will continue our reconnection experiment to investigate these parameters in detail in our future work.

References

[1] Giovanelli R G 1946 *Nature* **158** 81
[2] Baker D N, Pulkkinen T I, Angelopoulos V et al 1996 *J. Geophys. Res.* **101** 12975
[3] Priest E and Forbes T 2000 *Magnetic Reconnection: MHD Theory and Applications* (Cambridge: Cambridge University Press)
[4] Vasyliunas V M 1975 *Rev. Geophys. Space Phys.* **13** 303
[5] Birn J, Drake J F, Shay M A et al 2001 *J. Geophys. Res.* **106** 3715
[6] Huang J and Ma Z W 2008 *Chin. Phys. Lett.* **25** 1764
[7] Øieroset M, Phan T D, Fujimoto M et al 2001 *Nature* **412** 414
[8] Fu X R, Lu Q M and Wang S 2006 *Phys. Plasmas* **13** 012309
[9] Huang C, Lu Q M and Wang S 2010 *Phys. Plasmas* **17** 072306
[10] Lu Q M, Huang C, Xie J L et al 2010 *J. Geophys. Res.* **115** A11208
[11] Lu Q M, Wang R S, Xie J L et al 2011 *Chin. Sci. Bull.* **56** 1174
[12] Wang R S, Lu Q M, Huang C et al 2010 *J. Geophys. Res.* **115** A01209
[13] Lai X S, Zhou M, Deng X H et al 2015 *Chin. Phys. Lett.* **32** 095202
[14] Daughton W, Scudder J and Karimabadi H 2006 *Phys. Plasmas* **13** 072101
[15] Drake J F, Swisdak M, Schoeffler K M et al 2006 *Geophys. Res. Lett.* **33** L13105
[16] Wang R S, Lu Q M, Du A M and Wang S 2010 *Phys. Rev. Lett.* **104** 175003
[17] Wang R S, Lu Q M, Nakamura R et al 2016 *Nat. Phys.* **12** 263
[18] Phan T D, Eastwood J P, Shay M A et al 2018 *Nature* **557** 202
[19] Wang R S, Lu Q M, Nakamura R et al 2018 *Geophys. Res. Lett.* **45** 4542
[20] Gregory G H 2018 *Phys. Plasmas* **25** 055501
[21] Yamada M, Kulsrud R and Hantao Ji 2010 *Rev. Mod. Phys.* **82** 603
[22] Stenzel R L and Gekelman W 1979 *Phys. Rev. Lett.* **42** 1055
[23] Wild N, Gekelman W and Stenzel R L 1981 *Phys. Rev. Lett.* **46** 339
[24] Yamada M, Ono Y, Hayakawa A et al 1990 *Phys. Rev. Lett.* **65** 721
[25] Ren Y, Yamada M, Gerhardt S et al 2005 *Phys. Rev. Lett.* **95** 055003
[26] Yoo J, Yamada M, Ji H et al 2013 *Phys. Rev. Lett.* **110** 215007
[27] Dong Q L, Wang S J, Lu Q M et al 2012 *Phys. Rev. Lett.* **108** 215001
[28] Lu S, Lu Q M, Dong Q L et al 2013 *Phys. Plasmas* **20** 112110
[29] Frank A G, Bogdanov S Y, Markov V S et al 2005 *Phys. Plasmas* **12** 052316